

First Principles Study of Collector Transit Time Modulation in Double Heterojunction Bipolar Transistors

Jonathan P. Sculley¹, Yihao Fang², Brian Markman², Miguel E. Urteaga³, Andy D. Carter³, Mark J. W. Rodwell² and Paul D. Yoder¹

¹School of Electrical and Computer Engineering, Georgia Institute of Technology, Atlanta, 30332, USA

²Department of Electrical and Computer Engineering, University of California, Santa Barbara, 93106, USA

³Teledyne Scientific and Imaging, 1049 Camino Dos Rios, Thousand Oaks, CA, 91360, USA

Email: jonathan.sculley@gatech.edu / Phone: (678) 770-6610

Introduction: Velocity overshoot in heterojunction bipolar transistors has long been recognized to significantly reduce collector signal delay below that predicted under the assumption of a constant saturated electron velocity [1, 2]. This phenomenon has proven critical for high frequency operation of InP DHBTs which has resulted in cutoff frequencies above 1 THz [3]. In order to better understand the operation of these devices, we further explore the microscopic electron dynamics through simulation. We report modulated collector signal delay results from static and dynamic full band ensemble Monte Carlo simulation of a 300nm InGaAs/InP DHBT with a 300 nm collector.

Velocity Overshoot and Current Delay: Fig. 1 shows the band diagram and particle energies for two DC simulations: (a) low V_{cb} high $J_{n,e}$ and (b) high V_{cb} low $J_{n,e}$ near breakdown. In both cases, electrons injected into the collector from the base gradually gain energy and experience high drift velocity until reaching sufficient energy to enter the L-valley. Upon reaching this energy, the electrons scatter into satellite valleys and their velocity quickly saturates. Due to higher fields near the base, electrons in the high bias simulation reach this energy over a much shorter distance. Fig. 2a shows the average velocity profile at three different biasing levels along with the collector signal delay integrand first elucidated by Laux [1]. The collector signal delay integrand is disproportionately affected by velocity overshoot due to its dependence on inverse velocity and a weighting factor maximum near the base. The level of electron current injection from the base ($J_{n,e}$) also significantly affects electron velocity as shown in Fig. 2b. Large $J_{n,e}$ results in a negative charge throughout the collector, causing a negative electric field slope. This leads to stronger fields near the sub-collector and weaker fields near the base. The weaker electric field near the base results in a wider region of velocity overshoot and a significant reduction in collector signal delay. The dependence of collector current delay on both V_{cb} and $J_{n,e}$ is shown in Fig. 3.

Dynamic Simulations: Under sinusoidal stimulation, these effects combine on the load line such that current delay is minimum near the knee voltage and maximum near breakdown. This results in significant transit time modulation. Fig. 4 illustrates this in the time-domain whereby a large signal delay is observed at the minimum current point and a much smaller delay is seen at the maximum current point. This collector signal delay modulation can also be observed by re-forming the traditional weighted average transit time positional integral into a per-particle weighted transit time integral which is more suited for understanding dynamic device operation:

$$\tau_i^w = \int_0^{\tau_i} \left(1 - \frac{x_i(t)}{W_c} \right) dt$$

Here τ_i is the unweighted particle transit time, and W_c is the collector width. Each point in Fig. 5 represents the weighted transit time of a single particle, and this illustrates more clearly how the collector current delay is modulated by V_{cb} and $J_{n,e}$. The average weighted particle transit time shown in Fig. 5 is also similar to the collector signal delays from the DC simulations in Fig. 2: ~0.5 ps at $V_{cb} = 1$ V and $J_{n,e} = 1$ mA/ μm^2 , and ~1.8 ps at $V_{cb} = 8.5$ V and $J_{n,e} < 0.1$ mA/ μm^2 . The Fourier transform of the injected current and the collector current shown in Fig. 6 further illustrates the spectral content introduced in the collector current because of collector signal delay modulation.

Conclusions: In conclusion, we have presented static and dynamic transit times for a 300 nm InP DHBT determined by Monte Carlo simulation. In addition, we have presented an original time-domain formulation of the collector signal delay equation which has great utility for understanding the physics of dynamic transit time modulation. We show that transit time modulation due to space charge screening during each full period can represent a very large fraction of the average transit time during normal device operation and that it can occur before the onset of the Kirk effect.

[1] Laux, S.E. *et al.*, *IEEE Elec. Dev. Lett.* 11, 174 (1990) [2] Ishibashi, T., *IEEE Trans. On Elec. Dev.* 37, 2103 (1990)
[3] Urteaga, M. *et al.*, *69th Dev. Res. Conf.*, 281 (2011)

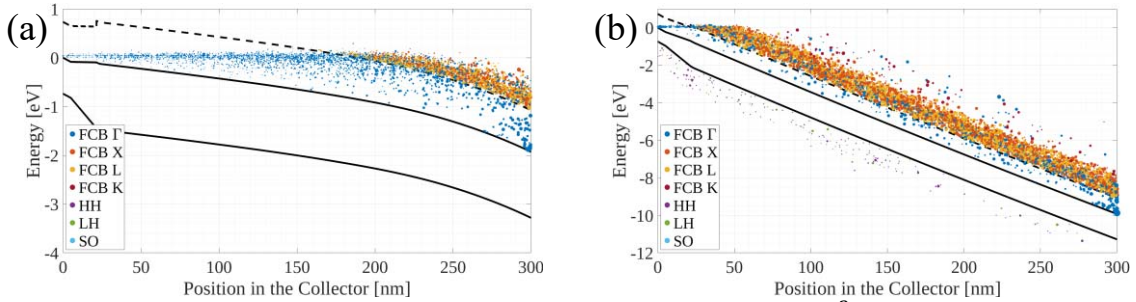


Fig. 1. Band diagram for two DC simulations: (a) $V_{cb} = 1$ V, $J_{n,e} = 1$ mA/ μm^2 , and (b) near breakdown with $V_{cb} = 9$ V, $J_{n,e} = 0.001$ mA/ μm^2 . Each dot represents a single simulation particle, and the dashed line represents the L-valley minimum energy. Velocity overshoot occurs until electrons reach the L-valley after approximately 180 nm (a) and 30 nm (b).

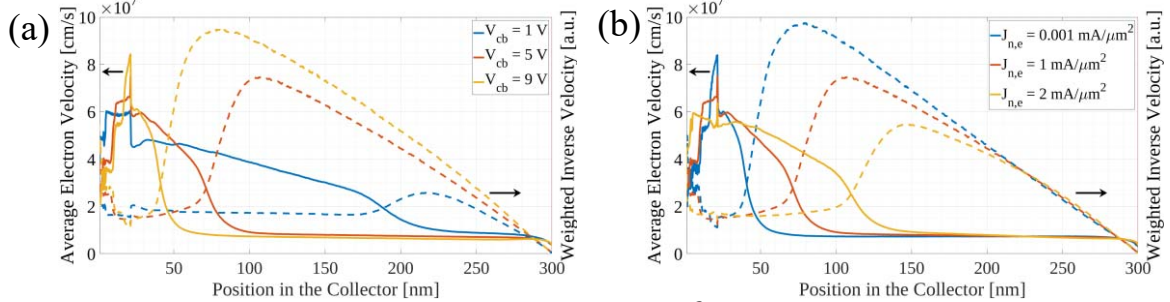


Fig. 2. Comparison of DC velocity profiles for $J_{n,e} = 1$ mA/ μm^2 (a) and $V_{cb} = 5$ V (b) for different values of V_{cb} and $J_{n,e}$, respectively. Velocity overshoot occurs over a wider region for lower biases and higher injection levels. The dashed line is collector signal delay integrand which is proportionally to the inverse of average electron velocity multiplied by the weighting factor of $1 - x/W_c$ where W_c is the collector width (300 nm).

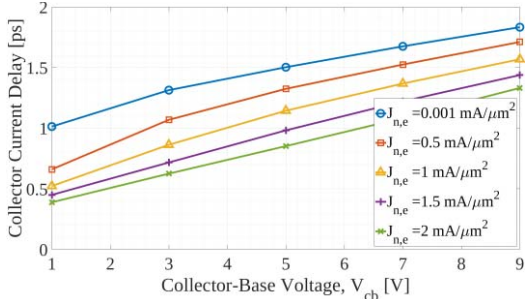


Fig. 3. DC collector signal delay variation with V_{cb} and $J_{n,e}$. The effects of varying both V_{cb} and $J_{n,e}$ combine in AC resulting in collector signal delay extremes at either end of the load line.

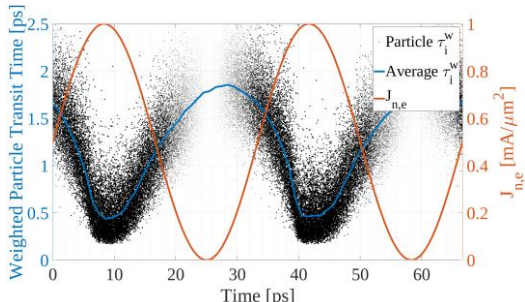


Fig. 5. Weighted particle transit times vs. the time of their injection into the collector for an AC simulation with $V_{cc} = 9$ V. The size of each dot represents the amount of charge associated with that particle.

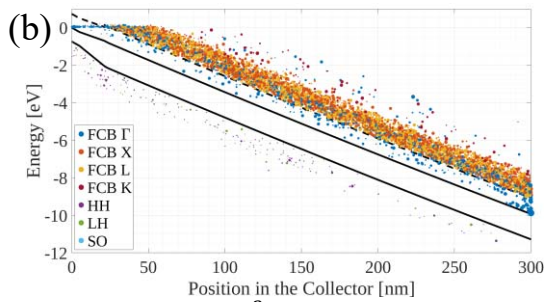


Fig. 4. AC injected current and collector current vs. time for $V_{cc} = 9$ V. $J_{c,\text{particle}}$ is the contribution to collector current from particle motion while J_{total} also includes displacement current.

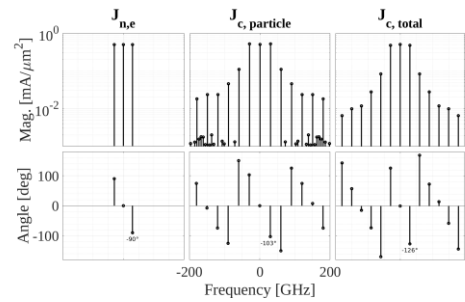


Fig. 6. FFT magnitude and angle for injected current, collector current contributed by particle motion, and total collector current including displacement current. The higher frequencies in the collector current are due to collector signal delay modulation.